Molten Salt Thermal Energy Storage Materials for Solar Power Generation

Ramana G. Reddy
ACIPCO Endowed Professor
Department of Metallurgical and Materials Engineering,
The University of Alabama, Tuscaloosa, AL 35487-0202, USA

Abstract: Concentrating solar power (CSP) technologies are seen as the Solar Program's most attractive option for meeting utility-scale needs. Innovative research and development activities that will reduce the cost of CSP plants and facilitate their implementation are of prime consideration. Two key opportunities for cost reduction are the development of improved heat transfer fluids and improved methods for thermal storage. This presentation will deal with our research on development of low melting point (LMP) molten salt thermal energy storage media with high thermal energy storage density for sensible heat storage systems. The essential properties of the selected LMP molten salts for thermal storage in solar energy applications are including melting point, heat capacity, density, and thermal energy storage capacity. To develop candidate low melt point salt materials, we used thermodynamic modeling calculations to estimate eutectic compositions of the salt mixtures, heat capacities and densities. Material properties were validated by using experimental techniques including DSC, TGA and other characterization techniques. The energy storage density of new TES molten salts identified are well above the current solar salt. All salt mixtures have melting temperatures in the range of 89-124°C, and energy storage density from 1099 MJ/m3 to 1242 MJ/m3 which is a 45-64% improvement over the current solar salt (756 MJ/m3).

Key words: Molten salts, Thermodynamic modeling, Energy density, Melting point

1. Introduction

The rate of solar energy intercepted by the planet is 170 trillion kW, about 5,000 times greater than the sum of all other energy sources, but 30% is reflected to space and 47% is used for evaporation. Less than 0.5% is represented in the kinetic energy of the wind, waves, and in photosynthetic storage in plants. The average daily solar radiation falling upon one acre in the continental United States is equivalent in total energy content to about eleven barrels of oil. Reusable energy of this quantity represents a huge, useful, and relatively unexploited energy supply [1, 2].

The intermittent character of solar energy requires a Thermal Energy Storage (TES) system for the most effective utilization of this energy source. The TES system serves as a reservoir of energy to collect and transfer thermal energy from the Heat Transfer Fluid (HTF) to storage media. Depending upon how the energy is transferred, there are basically three kinds of systems - sensible heat storage (SHS) which utilizes the specific heat or sensible heat of the storage media, latent heat storage (LHS) which involves storing and recovering heat through the solid-liquid phase change materials (PCMs) and thermochemical heat storage (TCHS) which involves storing heat from the materials heat capacity and its change as function of temperature accompanied with chemical reaction. The materials chemical bonds are broken due to chemical reactions in the TCHS process. This results in charging and discharging process not

completely reversible, which reduces the stability and recyclability of storage operation. The sensible heat storage (SHS) option is adopted by most commercial TES systems due to its simplicity in heat exchange steps [3-5]. Molten salts are used as the HTF and storage medium for power towers and mineral oils are used mostly in parabolic trough systems. However, the energy conversion efficiency in these applications are limited because mineral oils have low heat transfer and storage capacities per unit volume and restricted operating temperature range. The search for better heat storage materials has recently been focused on the use of low melting point (LMP) molten salts in order to avoid the above-mentioned problem.

A wide variety of equipment is available to capture solar energy and use it for space and water heating, and for electricity generation. The three systems are: solar parabolic trough, solar tower and solar dish. Parabolic trough is constructed by silver coated parabolic mirror and there is a Dewar tube going through the length of the mirror and set on the focal point, all the radiation is concentrated on the tube and transfer by heat transfer fluid (HTF) to the thermal energy storage unit. Solar tower are used to capture solar energy with thousands of mirrors and focus the concentrated sunlight to the top of the tower which is located in the middle of the heliostats. The thermal energy storage medium within the tower was heated to high temperature and transferred to thermal energy storage tank and eventually sent to steam generator. The solar dish is built with a large, reflective parabolic dish which concentrates all the received sunlight to one spot. There is normally a receiver located on the focal point and transform the solar energy to other forms of useful energy. The working upper limit temperature of solar parabolic trough system is the lowest among these three systems, normally its maximum working temperature is within the range from 400-500°C; the solar tower has higher maximum working temperature which ranges from 500-1000°C; the solar dish has the highest working upper limit temperature which reaches 700-1200°C [4].

The three major components of solar thermal energy utilization systems are the solar collector, the energy storage system, and the steam generator used for the turbine-electric generator. Thermal energy is usually collected by a parabolic trough, transferred to thermal storage by a heat transfer fluid, and then transferred to a steam generator by storage media. For active thermal energy storage in a direct system, the heat transfer fluid collects the solar heat and also serves as storage medium. The solar energy system costs are strongly dependent on the properties of the thermal storage media and the heat transfer fluid. To achieve high thermal conversion efficiency, sensible, latent thermal storage and therochemical storage systems require that the heat transfer fluid possess several important characteristics, such as a wide liquid temperature range, high thermal stability and high storage density. In particular, an operating temperature higher than 400^{o}C in a parabolic trough system would greatly enhance the thermal cycle efficiency.

The energy conversion efficiency is the most concerned parameter in the solar energy storage application and the theoretical and real engineering efficiency are given in Fig. 1 as function of temperature. The theoretical conversion efficiency can be up to 80% while in real application, the value is always less than 60% regardless of collectors. The actual efficiency increases with temperature in the whole working temperature. As a result of that, the thermal energy storage materials in solar parabolic trough, for instance, should be able to work stably at the upper limit temperature of this type of collection system which is 500^{o}C to ensure the highest efficiency [4, 5].

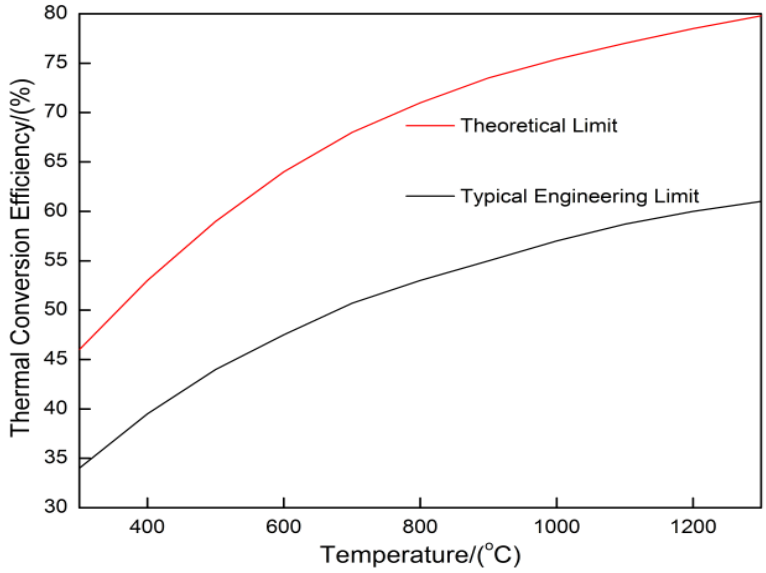

Fig. 1 Theoretical and engineering energy conversion efficiency as function of temperature

Thermal Storage Media and Heat Transfer Fluids

For most industrial applications, water is the most popular heat transfer fluid [6]. It has high latent thermal energy, high thermal conductivity, high specific heat, and high density with moderate viscosity. The primary drawback with water as a heat transfer fluid is the limited range of temperature over which it can be used. The theoretical liquid range of water is between 0°C and 100°C, but the practical temperature range for water used as heat transfer fluid is much less than 100°C, because of the high vapor pressure near the boiling point. The extension of the application temperature range to below the freeze point can be accomplished by using antifreeze (e.g. ethylene glycol-water mixture), but the extension over the boiling point for aqueous system is extremely difficult. Also, high pressure is needed to keep water at a liquid state when the temperature is over 100°C, which results in high costs due to the related pressure vessels and pipes. Accordingly, high temperature water (over 100°C) is unsuitable as a heat transfer fluid or thermal energy storage medium for solar energy power plants.

Gases are sometimes used as heat transfer fluids instead of water when a wider temperature range is required. However, gases have low density, low specific heat capacity and low thermal conductivity. These properties cause gaseous heat transfer fluids to be not as effective as liquids. A gaseous heat transfer fluid is usually used only when a liquid cannot be used, as in applications requiring very high temperatures.

Thermal oils can maintain their liquid phase up to about 300°C, and can be used as thermal storage media and heat transfer fluids, but their applications are limited by several intrinsic disadvantages such as low decomposition temperature, low density, flammability, high vapor pressure, fuming tendency, and low chemical stability [7]. Santotherm 55 is common thermal oil used as thermal storage medium and heat transfer fluid. It allows working temperatures above 300°C without decomposing, and its main properties are listed in Table 1. One of the main characteristics of this oil is its low thermal conductivity. Furthermore, its density is highly dependent on its temperature,

which permits the use of just one storage tank to contain both the hot and the cold oil in thermal stratification (the thermocline effect). An inlet field temperature of 210^{o}C and an outlet field of 290^{o}C are obtained. The main disadvantages of this thermal oil are low density, low heat capacity, and low decomposition temperature, resulting in low energy storage.

Table 1. Main Properties of Santotherm 55 Thermal Oil at 25^{o}C.

Properties	Values
Density ρ_f, kg/m^3	886.2
Specific heat capacity C_p, J/g. K	1.907
Thermal conductivity k, W/m. K	0.1891
Dynamic viscosity μ, Pa S	0.0105
Prandlt number Pr	160.5

Ionic liquids have emerged as novel thermal storage and heat transfer fluids for low to medium temperature applications in sensible heat storage systems [8]. Ionic liquids are salts, usually having low melting points. Their important properties include extremely low volatility in the liquid state, non-flammability, relatively wide temperature range, and large number of possible compositions allowing fine-tuning of ionic liquid properties for specific applications. The melting temperature and thermal decomposition temperature of selected ionic liquids have been summarized [6-11]. For example, [BF_4] and [Tf_2N] ionic liquids have a wide liquid temperature range and exhibit possible thermal stability up to 400^{o}C. However, most ionic liquids with chloride anions have onset decomposition temperatures lower than 300^{o}C. For application as TES media, ionic liquids have a limited operating temperature range although they have higher thermal storage density capacities (higher enthalpy changes as a function of temperature). It has also been reported that ionic liquids with chloride anions are moisture sensitive and have high corrosivity on common steel alloys [9], and limited cycle life and lower decomposition temperatures which limits their possible application.

Liquid metals and molten salts have been proposed as heat transfer fluids for high temperatures from 250 to 1000^{o}C [12-15]. Due to the avoidance of high pressure, the wall thickness requirements of the piping, pump casings, heat exchangers, and other equipment were much lower than those required for high-pressure steam systems operating in this temperature range. One problem with liquid metals and molten salts is that the heat exchanger system has to be preheated, since when temperatures are not high enough, metals and molten salts can freeze. Liquid metals are not viable candidates for energy storage media for concentrated solar power (CSP) due to a combination of high cost, relatively high melting point, and high vapor pressure at the operating temperature. A liquid metal heat transfer medium was commercialized in 1923 [16] and a molten salt heat transfer medium was commercialized in 1937 [17]. Although there are some operational problems as described above, molten salts have been used in cracking units in the petroleum refining industry. The reason is that there is no better heat transfer medium available. The molten salt medium usually is a mixture of sodium nitrite, sodium nitrate, and potassium nitrate.

Current molten salt heat transfer fluid and thermal storage media are a mixture of 60% $NaNO_3$ and 40% KNO_3 [18]. The liquid temperature range is 220-600^{o}C. The main disadvantage of this salt mixture is the high melting point. In the evening, and especially in winter, the salt can freeze and block the pipeline. In order to overcome this problem,

auxiliary facilities need to be installed, which could increase the investment and operational costs. Evaluation of several salt compounds based on requirements for TES systems (thermal stability, vapor pressure, freezing point, specific gravity, heat capacity, viscosity, chemical compatibility with steels, thermal energy storage density, and recyclability), resulted in the identification of a promising candidate LMP molten salt system, viz., nitrates such as KNO_3, $LiNO_3$, $NaNO_3$ and nitrites such as $NaNO_2$ and KNO_2. Within these systems, several ternary and quaternary eutectic liquid compositions with eutectic melting temperatures in the range of 79-116°C were identified. These melting points can be further lowered by the addition of one or more $ABNO_3$ nitrate compounds where A and B are cations. Common metal and molten salt heat transfer media and their properties are listed in Table 2 [19]. Little to no fundamental data on the physico-chemical properties of these systems at the required operating conditions is available at present.

Table 2. Common Metal and Molten Salt Heat Transfer Media and Their Properties

Heat Transfer Medium	Melting point (°C)	Density (g/cc)	$\Delta_f H°$ (kJ/mol)
Li	180	0.53	0
Na	97.8	0.97	0
K	63.7	0.86	0
$LiNO_3$	253	2.38	-483.1
$NaNO_3$	306.5	2.26	-467.9
KNO_3	334	2.10	-494.6
$NaNO_2$	280	2.17	-354.6
KNO_2	437	1.91	-365.9
$Mg(NO_3)_2$	---	2.30	-790.7
$Ca(NO_3)_2$	561	2.50	-938.2
$Sr(NO_3)_2$	570	2.99	-978.2
$Ba(NO_3)_2$	590	3.24	-988.0

This paper presents development and synthesis of newer low melting point molten salt mixtures with freezing point lower than those currently used for thermal energy storage applications. The approach to develop lower melting point molten salt mixtures is by thermodynamic modeling to predict new eutectic mixtures followed by experimental verification of the predicted eutectic temperatures of the eutectic compositions. The new systems with simulated eutectic compositions were tested for their experimental melting points, heat capacities and density. Some significant thermodynamic properties such as heat capacity, enthalpy, and entropy and Gibbs energy were calculated to evaluate the energy change of the system in the phase change process and the potential of being applied in the parabolic trough solar power plant. The energy density was obtained by using the experimental measured melting point, density and heat capacity of the mixtures in molten state. Finally, nine down-selected systems are present and discussed in this article.

2. Thermodynamic Modeling

Thermodynamic model was introduced to predict the eutectic temperature of salt systems based on the Gibbs energies of fusion of individual salt and that of mixing of constituent binary systems. At the eutectic temperature, the Gibbs energies in the liquid state and solid state of salt are equal [19]. In thermodynamics, Gibbs energy of fusion can be expressed by the equation given as follows:

$$\Delta G = \Delta H - T\Delta S \qquad [1]$$

where ΔH is the change of enthalpy of fusion and ΔS is the change of entropy of fusion. Equally, the entropy change of fusion can be expressed by differentiating ΔG and the equation is given:

$$\frac{d\Delta G}{dT} = -\Delta S \qquad [2]$$

It is known that the change in entropy can be expressed in terms of change in heat capacity in the melting process as:

$$\frac{d\Delta S}{dT} = \frac{\Delta C_p}{T} \qquad [3]$$

If the change of heat capacity is assume to be independent of temperature, the integral of ΔS from Tm to T can be shown as:

$$\Delta S = \Delta S_m + \Delta C_p ln\left(\frac{T}{T_m}\right) \qquad [4]$$

where ΔSm is the entropy of fusion at the melting point which is equal to $\Delta H_m/T_m$. Accordingly, Eq.4 can be rewritten as:

$$\Delta S = \frac{\Delta H_m}{T_m} + \Delta C_p ln\left(\frac{T}{T_m}\right) \qquad [5]$$

Substituting Eq. 5 in Eq. 2 and integrating the equation from T_m to T we get,

$$\Delta G_f = \frac{H_m}{T_m}(T_m - T) - \Delta C_p \left[T ln\left(\frac{T}{T_m}\right) + T_m - T\right] \qquad [6]$$

Eq. 6 illustrates that by using the change of heat capacity, melting point and enthalpy of fusion, the Gibbs energy change at any temperature can be obtained.

The standard Gibbs energy of fusion of a salt '1' can be expressed in terms of the activity of the salt as:

$$\Delta G_1^{\circ} = -RTln(a_1) = -RTln(X_1) - RTln(\gamma_1)$$

$$= -RTln(X_1) - \bar{G}_1^{xs} \qquad [7]$$

where $\bar{G}_1^{xs}$ is the molar excess Gibbs energy and X_1 is the molefraction of the salt '1'. Gibbs energy of fusion at any give temperature T is expressed by Eq 7 in terms of its molefraction and partial molar excess Gibbs energy.

Taking the ternary system, $LiNO_3$-$NaNO_3$-KNO_3, as an example in which the integral molar excess Gibbs energy is composed of the summation of the Gibbs energies of three constituent binary systems and one ternary. The expression of the integral excess Gibbs energy is given by Eq.8.

$$G^{xs} = G_{1-2}^{xs} + G_{2-3}^{xs} + G_{1-3}^{xs} + G_{1-2-3}^{xs} \qquad [8]$$

Gibbs energies of the three constituent binary systems, $LiNO_3$-$NaNO_3$, $LiNO_3$-KNO_3, and $NaNO_3$-KNO_3 of the $LiNO_3$-$NaNO_3$-KNO_3 ternary system are taken from the literature [20, 21]. The Gibbs energies of mixing or the

integral excess Gibbs energies of the three constituent binary systems of the $LiNO_3$-$NaNO_3$-KNO_3 ternary system are given below:

$LiNO_3$-$NaNO_3$ Binary System

$$G^{xs}_{LiNO_3-NaNO_3} = X_{LiNO3}\, X_{NaNO3}[-18910 - 27.51\, T\, ln(T) + 205.27\, T]\ J/mol \qquad [9]$$

$LiNO_3$-KNO_3 Binary System

$$G^{xs}_{LiNO_3-KNO_3} = X_{LiNO3}\, X_{KNO3}[-5310 - 6.01\, T\, ln(T) + 30.5\, T]\ \text{J/mol} \qquad [10]$$

$NaNO_3$-KNO_3 Binary System

$$G^{xs}_{NaNO_3-KNO_3} = X_{NaNO\ 3}\, X_{KNO\ 3}[-1709.2 - 284.5\, X_{NaNO\ 3}]\ \text{J/mol} \qquad [11]$$

When assume the intergral excess Gibbs energy of G^{xs}_{1-2-3} to be zero, the excess Gibbs energy in the ternary system can be expressed by the summation of three constituent binary systems:

$$G^{xs} = G^{xs}_{LiNO_3-NaNO_3} + G^{xs}_{NaNO_3-KNO_3} + G^{xs}_{LiNO_o-KNO_3} \qquad [12]$$

Generally, the partial molar excess Gibbs energies are reduced from the integral molar excess Gibbs energy and can be expressed by the generalized equation for certain "m" component salt as:

$$\bar{G}^{xs}_i = G^{xs} + \sum_{j=2}^{m}\left(\delta_{ij} - X_j\right)\frac{\delta G^{xs}}{\delta X_j} \qquad [13]$$

In the ternary system, the i value equals to 1,2 and 3, and the partial molar excess Gibbs energy of mixing for each component can be expressed as follows:

$$\bar{G}^{xs}_1 = G^{xs} - X_2\frac{\partial G^{xs}}{\partial X_2} - X_3\frac{\partial G^{xs}}{\partial X_3} \qquad [14]$$

$$\bar{G}^{xs}_2 = G^{xs} + (1 - X_2)\frac{\partial G^{xs}}{\partial X_2} - X_3\frac{\partial G^{xs}}{\partial X_3} \qquad [15]$$

$$\bar{G}^{xs}_3 = G^{xs} - X_2\frac{\partial G^{xs}}{\partial X_2} + (1 - X_3)\frac{\partial G^{xs}}{\partial X_3} \qquad [16]$$

Based on Eq. 7 and the partial molar excess Gibbs energies of individual components, the Gibbs energies of fusion for the three components can be expressed as Eq. 17-19.

$$\Delta G^{\circ}_{LiNO_3} = -RTln\left(X_{LiNO_3}\right) - \bar{G}^{xs}_{LiNO_3} \qquad [17]$$

$$\Delta G^{\circ}_{NaNO_3} = -RTln\left(X_{NaNO_3}\right) - \bar{G}^{xs}_{NaNO_3} \qquad [18]$$

$$\Delta G^{\circ}_{KNO_3} = -RTln\left(X_{KNO_3}\right) - \bar{G}^{xs}_{KNO_3} \qquad [19]$$

The fusion of the ternary salt system is defined by solutions of Eqs 17-19. Newton-Raphson method can be used to solve these three non-linear equations by linearizing the non-linear equations using the Taylor series and truncating the

series to first order derivatives. Consider the three non-linear functions F, G, and H in three variables, x, y, and z. The three equations that are solved for the three variables are written as:

$$F(x, y, z) = 0;$$

$$G(x, y, z) = 0;$$

$$H(x, y, z) = 0; \quad [20]$$

The partial derivatives of the function F with respect to x, y and z are given as:

$$F_x = \frac{\partial F}{\partial x}; F_y = \frac{\partial F}{\partial y}; F_z = \frac{\partial F}{\partial z}; \quad [21]$$

Similarly, the partials derivatives can be expressed for the other two functions G and H.

Newton-Raphson iterative method of solving the three equations in three variables essentially deals with the solution of the incremental vector in the matrix equation given below.

$$\begin{bmatrix} F_x & F_y & F_z \\ G_x & G_y & G_z \\ H_x & H_y & H_z \end{bmatrix} \begin{bmatrix} \Delta x \\ \Delta y \\ \Delta z \end{bmatrix} = - \begin{bmatrix} F(x_i, y_i, z_i) \\ G(x_i, y_i, z_i) \\ H(x_i, y_i, z_i) \end{bmatrix} \quad [22]$$

For the initial values of x, y, and z, (say x_i, y_i, and z_i) the right hand side vector contains the values of the functions at the initial values (x_i, y_i, and z_i). The 3×3 matrix on the left hand side contains the partial derivatives of the functions with respect to the three variables at the initial values. Solutions of the matrix equation (Eq. 22) result in the increments of the variables Δx, Δy, and Δz. The variables for the next iteration will then be $x_i + \Delta x$, $y_i + \Delta y$, and $z_i + \Delta z$. The process of solving the matrix equation (Eq. 22) is continued until the increments in the variables Δx, Δy, and Δz is less than a very small quantity. The iteration process is then said to be converged and the values of the variables at convergence of the solution are the roots of the system of the three fusion equations.

The composition of $LiNO_3$, $NaNO_3$ and KNO_3 and the eutectic temperature is solved by using the Newton-Raphson iterative method. The predicted eutectic temperature for the $LiNO_3$-$NaNO_3$-KNO_3 ternary system was 116°C and the eutectic composition was 25.92 wt% $LiNO_3$, 20.01 wt% $NaNO_3$, and 54.07 wt% KNO_3. The similar method is applied to other multi-component systems to determine the eutectic compositions and temperatures. The predicted melting points for new solar energy storage system are given Table 3.

Table 3. Calculated composition and melting point of multi-component molten salts systems

Salt #	System	Calc. T_{mp} (°C)
Salt #1	$LiNO_3$-$NaNO_3$-KNO_3	116.0
Salt #2	$NaNO_3$- $NaNO_2$- KNO_3	123.8
Salt #3	$LiNO_3$- $NaNO_3$- KNO_3-MgKN	98.6
Salt #4	$LiNO_3$- $NaNO_3$- KNO_3- $NaNO_2$	98.6
Salt #5	$LiNO_3$- $NaNO_3$- $NaNO_2$-KNO_3- KNO_2	95.7
Salt #6	$LiNO_3$-$NaNO_3$-KNO_3-KNO_2	100.0

Salt #7	$LiNO_3$-KNO_3-$NaNO_2$-KNO_2	108.1
Salt #8	$LiNO_3$-KNO_3-$NaNO_2$-$Mg(NO_3)_2$	100.8
Salt #9	$LiNO_3$-$NaNO_3$-KNO_3-$Mg(NO_3)_2$-MgK	103.6

3. Experimental

3.1 Sample preparation

The systems were prepared by mixing the component salts with calculated compositions and all the component salts (purity ≥ 99%, Alfa Aesar) can be used as received without any pre-preparation. Weighted amount of nitrate and nitrite salts were taken in a stainless steel crucible and placed on a hot plate in an argon atmosphere. Temperature of the salt is measured with a K-type thermocouple immersed in the salt. The salt mixture was static heated to melt completely at 200°C and then cooled to ambient temperature until the salt solidifies to a white mass. After that, the salt was ground into powders using mechanical rolling, sealed and kept in the desiccators.

3.2 Measurement of properties

Differential scanning calorimetry (DSC) was used to determine the melting point of the salt mixtures. Heat flow and temperature can be recorded in the instrument with an accuracy of 0.0001 mW and 0.01 K respectively. The measurements were made under purified nitrogen atmosphere with a flow rate of 20cc/min and at a heating rate of 5 K/min. A low scanning rate was chosen to record the heat flow curve as function of temperature in order to improve the sensitivity of detection [22]. It helps to pick up any small endothermic peaks and also avoids the thermal resistance between the internal furnace and sample. Nine systems were chosen to test and the eutectic composition is already listed in Table 4.

The heat capacity of salt mixtures were also measured by using DSC and the same procedure as that of melting point determination is followed with an addition of ‘iso-scan-iso’ steps to the program after 5-cycle temperature scan. The ‘iso stage’ refers to isothermal holding at a particular temperature, ‘scan stage’ refers to the heat flow recording at a heating rate of 5 $K.min^{-1}$ up to a an increment of 25 K, followed by another isothermal holding stage. This is a standard procedure followed in the measurement of heat capacity of materials using the DSC equipment [22]. This procedure of heat capacity measurement has two advantages; (i) any heat fluctuations during the recording are avoided by the isothermal steps and (ii) any phase transition can be highlighted by the choice of temperature range. Small temperature scan range is chosen to avoid thermal resistance between device and testing sample. The upper limit for the Cp measurement was set to 623.15 K in our experiments. To get the value of molar heat capacity of the sample, heat flow curve for the baseline of the empty sample pan also needs to be obtained immediately following the identical “iso-scan-iso” steps which were used for the actual sample run. The difference of heat flow between the actual crimpled sample and the empty sample pan is the absolute heat absorbed by the test sample.

Density measurement was carried out with standard densitometer which has fixed volume. Initial weight of the densitometer is measured and noted. Salt composition, of which the density is measured, is placed in a beaker on a hot place. The densitometer is also placed on the same hot plate. The temperature is set to a fixed value above the melting point of the salt and is measured by a thermocouple. After the salt is melted and when the temperature shows stable

reading, the molten salt is poured in to the densitometer up to the set mark on the sensitometer bottle. The weight of the densitometer with the molten salt is measured. The weight difference between this weight and the weight of empty densitometer gives the weight of the molten salt at the fixed set temperature. By knowing the fixed volume in the densitometer, the density of the salt at that temperature can be calculated. This procedure is repeated at least three times to accurately determine the density of the salt.

The thermal stability at high temperature is a crucial parameter which determines the feasibility of the application of the new developed salt systems as heat transfer fluid. Thermal stabilities of the quaternary salt mixture were determined experimentally by using Perkin-Elmer TG/DTA instrument. In the short-term thermal stability measurement, small amount of the salt mixture was loaded and heated through 5 cycles at 10 °C/min from 30 °C to 500 °C and cooled at the same rate. The operation of the long-term thermal stability measurement is similar to the short term study. However, instead of heating and cooling sample continuously, the long-term thermal stability study was performed isothermally at constant temperature for 20 hours. The experiment was carried out at each temperature at an interval of 150°C in the temperature range of 200 – 500°C. Prior to the long-term thermal stability study, the salt mixture was dried at 150°C for 1 hour in argon atmosphere.

4. Results and Discussion

4.1 Melting point determination

All the selected systems are composed of alkaline nitrate and nitrite and most of them have three basic components which are lithium, sodium, potassium nitrate or nitrite. All the quaternary and quinary systems were developed on the basis of the $LiNO_3$-$NaNO_3$-KNO_3 baseline ternary. DSC plots for each system were collected for at least five runs (each run with fresh salt preparation) to ensure the reproducibility. Fig. 2 shows the typical DSC plot of the $LiNO_3$-$NaNO_3$-KNO_3 salt system.

It is observed that the first curve is different from last ones shown in the fig. 2 and this phenomenon is common for all the melting point measurement with DSC technique. This happened because in the first cycle, the moisture caught by salt mixture, especially the lithium nitrate, was removed in the process of heating. Moreover, the partially solidified sample in the sample loading process can be re-homogenized in the first heating cycle [23-25].

Table 4. DSC results of melting point, transition point and predicted melting point

Salt	System	T_{mp}			T_{trans}	ΔH_{fusion}
		Calculated, °C	Onset, °C	Peak, °C	Peak, °C	J/g
Salt #1	$LiNO_3$-$NaNO_3$-KNO_3	116.0	113.1	118.4	104.3	66.3
Salt #2	$NaNO_3$- $NaNO_2$- KNO_3	123.8	115.0	124.0	NA	9.7
Salt #3	$LiNO_3$- $NaNO_3$- KNO_3-MgKN	98.6	94.0	99.9	NA	24.4
Salt #4	$LiNO_3$- $NaNO_3$- KNO_3- $NaNO_2$	98.6	94.0	101.0	NA	6.0
Salt #5	$LiNO_3$- $NaNO_3$- $NaNO_2$-KNO_3- KNO_2	95.7	91.0	95.0	NA	6.2
Salt #6	$LiNO_3$-$NaNO_3$-KNO_3-KNO_2	100.0	93.0	96.0	NA	8.6
Salt #7	$LiNO_3$-KNO_3-$NaNO_2$-KNO_2	108.1	99.2	100.3	79.3	6.0

Salt #8	$LiNO_3$-KNO_3-$NaNO_2$-$Mg(NO_3)_2$	100.8	101.0	101.9	85.3	5.9
Salt #9	$LiNO_3$-$NaNO_3$-KNO_3-$Mg(NO_3)_2$-MgK	103.6	83.4	89.2	NA	9.3

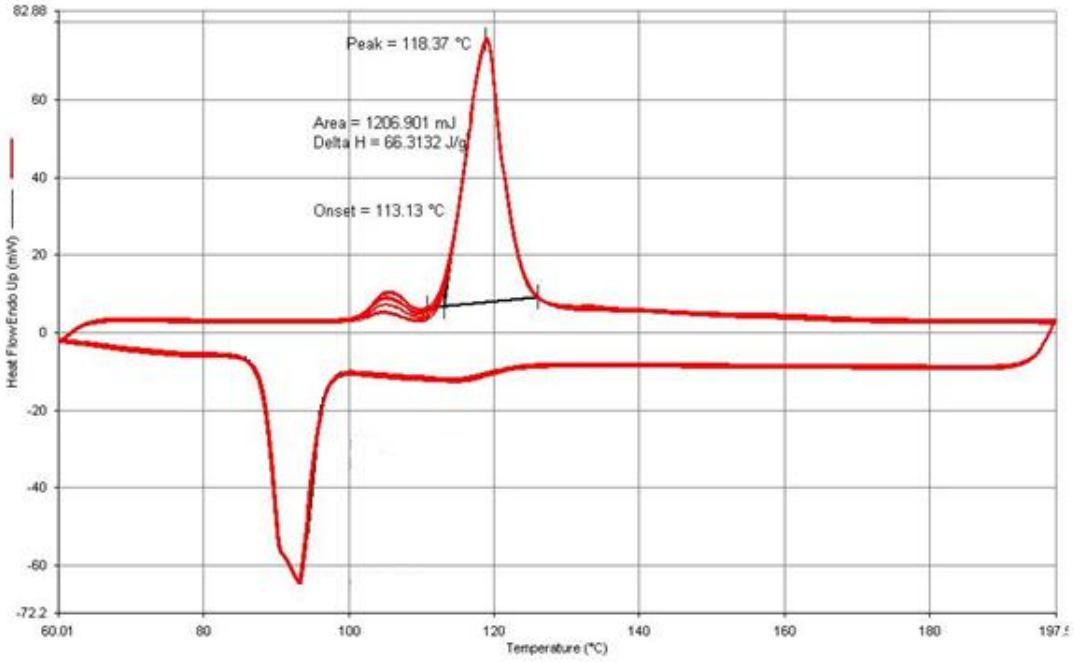

Fig. 2 DSC endothermic peaks of $LiNO_3$-$NaNO_3$-KNO_3 salt.

In salt #1, salt #7 and salt #8, more than one endothermic peak were observed. The first small endothermic peaks in the DSC plots of these salts refer to solid state phase transitions and the second large endothermic peaks refer to the melting of the salts. Normally, the onset temperature of transition is taken as the experimental transition point for any metallic sample. However, in case of molten salts mixtures, since the thermal conductivity is low [26-32], the complete transition is ensured only at the peak transition temperature. The thermal gradient which exists due to the low thermal conductivity of the salt results in internal heat flow which enhances the mixing in the salt. Thus, the transition temperature is defined as the peak temperature of phase transition. All the onset temperatures, peak temperatures, predicted temperatures, enthalpy of fusion for melting peaks and the solid phase transformation temperatures are given in Table 4. It is illustrated that the melting points of mixtures with lower or even no content of lithium nitrate turn out to be higher than those with sufficient amount of lithium nitrate. For most of the mixtures with melting point lower than 120^{o}C, the amount of lithium nitrate should be larger than 8.1wt%. Based on the observation above, it is concluded that the amount of lithium nitrate can play a significant role in lowering the melting point of salt mixture.

4.2 Heat capacity determination

In the heat capacity measurement, the heating process corresponds to collecting the value of required heat flow at each temperature. As a result of that all the heat capacity plots have the same shape with that of heat flow in the melting point measurements. Take the heat capacity plot of $LiNO_3$-$NaNO_3$-KNO_3 ternary system as an instance which is shown

in Fig. 3, the heat capacity curve also has two endothermic peaks happened at the same temperatures as those shown in Fig 2. Similarly, after the phase transformation, the heat capacity in liquid state becomes very stable and increase with temperature linearly with little slope.

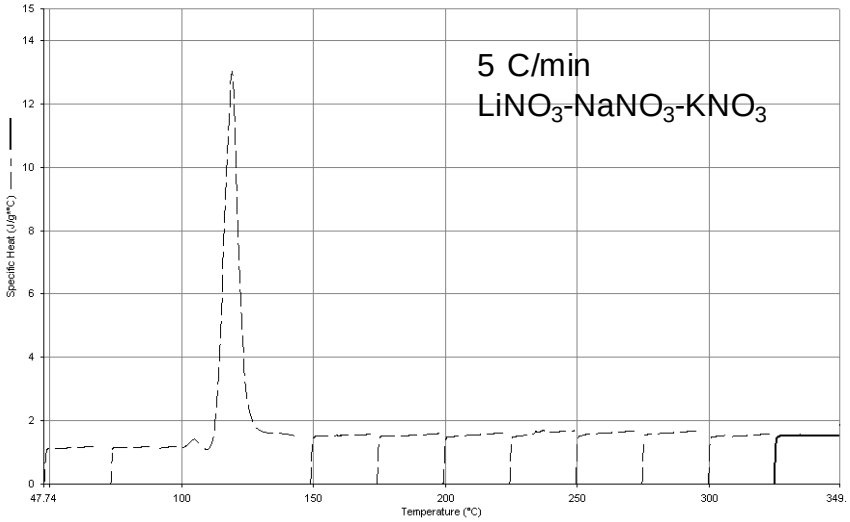

Fig. 3 Heat capacity data plot of $LiNO_3$-$NaNO_3$-KNO_3 ternary system as function of temperature

The heat capacity change as function of temperature for salt No. 1 was illustrated in Fig. 4. Since the change in the molar heat capacity of the salt in the liquid state is very small, the Cp data in the liquid state can be easily fit to an equation and extrapolated to higher temperatures. Similarly, heat capacity in liquid state for the rest eight new molten salt systems can also be fit into linear equation and extrapolated to the melting points. Table 5 shows the specific heat capacity of the all the salt mixtures measured at 623.15 K and extrapolated at 773.15K.

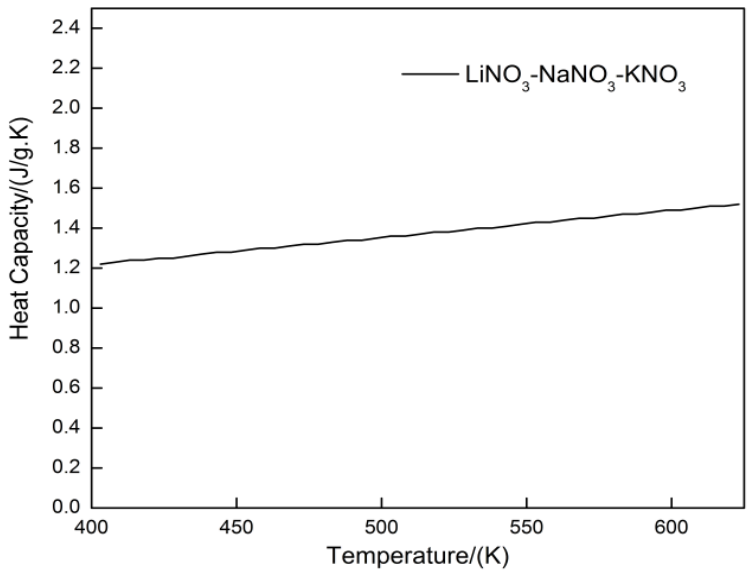

Fig. 4 Heat capacity of $LiNO_3$-$NaNO_3$-KNO_3 in liquid state

Table 5. Heat capacity of selected TES molten salt mixtures

Salt	System	Expt. (623.15K)	Extrapolated (773.15K)
		C_p, J/g.K	C_p, J/g.K
Salt #1	$LiNO_3$-$NaNO_3$-KNO_3	1.53	1.70
Salt #2	$NaNO_3$- $NaNO_2$- KNO_3	1.43	1.68
Salt #3	$LiNO_3$- $NaNO_3$- KNO_3-MgKN	1.48	1.55
Salt #4	$LiNO_3$- $NaNO_3$- KNO_3- $NaNO_2$	1.53	1.66
Salt #5	$LiNO_3$- $NaNO_3$- $NaNO_2$-KNO_3- KNO_2	1.53	1.70
Salt #6	$LiNO_3$-$NaNO_3$-KNO_3-KNO_2	1.51	1.63
Salt #7	$LiNO_3$-KNO_3-$NaNO_2$-KNO_2	1.56	1.67
Salt #8	$LiNO_3$-KNO_3-$NaNO_2$-$Mg(NO_3)_2$	1.55	1.68
Salt #9	$LiNO_3$-$NaNO_3$-KNO_3-$Mg(NO_3)_2$-MgK	1.61	1.70

4.3 Density determination

The density result of the salt as function of temperature is plotted for all the salts in Fig. 5 and Fig. 6. It is observed that the temperature dependence of density above the melting point is different from that in solid state. As known, in solid state, the density of salt has an exponential relation with temperature, while in these liquid cases the density values have linearly dependence with temperature. The liner variation as function of temperature allows the extrapolation of density at even higher temperature. All the results indicate that the density was decreased linearly as temperature increases and any specific density value in the molten state can be expressed by equation 4:

$$\rho = A\text{-}BT \qquad [23]$$

Where ρ (g/cm^3) is the density of salt, A (g/cm^3) is the initial density value at 0^{o}C and B (mg/cm$^{3\cdot}$°C) is the density change slope as function of temperature. The regression analysis is performed and the results for the coefficients are shown in Table 6. It is observed that the change of composition is implied on the coefficient A which indicates the initial point at 150°C. The temperature dependence coefficient B doesn't change much with composition, which may be mainly affected by the group of anion and cation.

Table 6. Coefficients A and B for density determination of the salts

Salt No.	System	A (g/cm^3)	B×10^3 (g/cm$^{3\cdot}$°C)
1	$LiNO_3$-$NaNO_3$-KNO_3	2.032	0.493
2	$NaNO_3$- $NaNO_2$- KNO_3	2.081	0.570
3	$LiNO_3$- $NaNO_3$- KNO_3-MgKN	2.055	0.526
4	$LiNO_3$- $NaNO_3$- KNO_3- $NaNO_2$	2.033	0.520
5	$LiNO_3$- $NaNO_3$- $NaNO_2$-KNO_3- KNO_2	2.018	0.485

6	$LiNO_3$-$NaNO_3$-KNO_3-KNO_2	2.060	0.554
7	$LiNO_3$-KNO_3-$NaNO_2$-KNO_2	2.048	0.554
8	$LiNO_3$-KNO_3-$NaNO_2$-$Mg(NO_3)_2$	2.044	0.524
9	$LiNO_3$-$NaNO_3$-KNO_3-$Mg(NO_3)_2$-MgK	2.060	0.566

In Fig. 5, all the density values are clustered around 1.98g/cm^3 at 150^{o}C to 1.86g/cm^3 at high temperature end and the deviation of density between all the mixtures is within in 0.047g/ cm^3. Among all the salt mixtures, the $NaNO_3$-$NaNO_2$-KNO_3 ternary system demonstrates the highest density value throughout the studied temperature range and $LiNO_3$-$NaNO_3$-KNO_3 ternary system, $LiNO_3$- $NaNO_3$-KNO_3-$NaNO_2$ quaternary system and $LiNO_3$-$NaNO_3$-KNO_3-$NaNO_2$-KNO_2 quinary system show densities at the bottom side of Fig. 5. For salt #2, which doesn't contain any lithium nitrate, the density at every selected temperature spot is obviously higher than that of salt #1, #4 and #5 which have large amount of lithium nitrate. Moreover, the salt #3 which contains the relatively small amount of lithium nitrate stays in between of salt #1 and salt #2. This comparison illustrates that the addition of lithium nitrate has an offsetting effect on density for molten salt and it is consistent with previous literature reports [33].

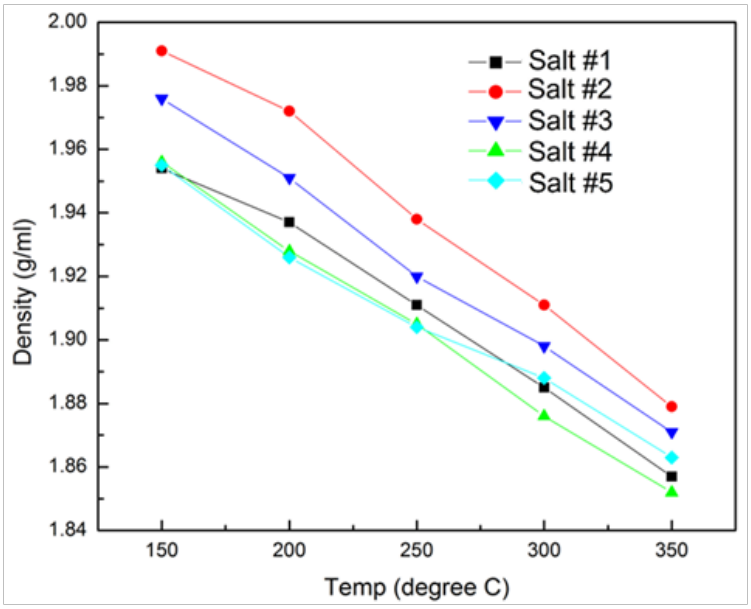

Fig. 5 The densities of the salt #1 to salt #5 as function of temperature

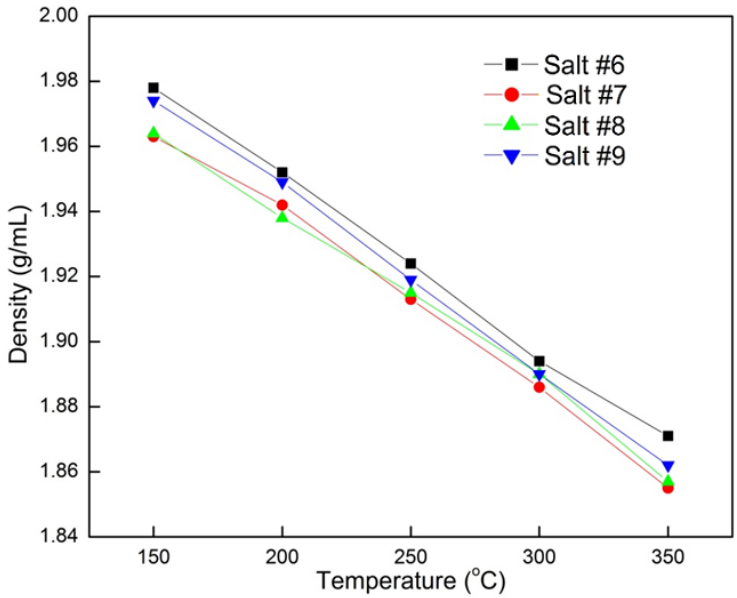

Fig. 6 The densities of the salt #6 to salt #9 as function of temperature

The four systems presented in Fig. 6 also show even closer density values in the studied temperature range. Similarly, salt #6 which contains the least lithium nitrate has the largest density. Salt #7 and salt #8 have almost same composition for the three dominating components, as a result of that, the density curves for both mixtures are determined by the same regression coefficient A and B. Moreover, the larger amount of lithium nitrate involved in these two salt mixtures contributes to the lower density given in Fig. 6, which further verifies the significantly offsetting effect of lithium nitrate on density.

4.4 Thermal energy storage capacity of molten salts

The energy density which is considered as one of the most significant parameters of TES application can be evaluated by calculation based on the measured density, heat capacity and working temperature range. The equation of the thermal energy storage capacity (E) at working temperature of 500°C is expressed in Eq. 24:

$$E = \rho \cdot Cp \cdot (500 - T_m) \qquad [24]$$

where Cp and ρ are heat capacity and density at 500°C, respectively, T_m is melting point for salt mixture. The extrapolation of density and heat capacity is based on the linear temperature dependence for both parameters in molten state and the values are shown in Table 7.

Table 7. Extrapolated value of density and heat capacity at 500°C of salt #1 to salt #9

Salt No.	System	Density (g/mL)	Heat Capacity (J/g.K)	Energy Density (MJ/m^3)
1	$LiNO_3$-$NaNO_3$-KNO_3	1.785	1.70	1162
2	$NaNO_3$- $NaNO_2$- KNO_3	1.796	1.68	1135
3	$LiNO_3$-$NaNO_3$-KNO_3-MgK	1.773	1.55	1099
4	LiNO3- NaNO3- KNO3- NaNO2	1.792	1.66	1189
5	$LiNO_3$- $NaNO_3$- $NaNO_2$-KNO_3- KNO_2	1.796	1.70	1232
6	$LiNO_3$-$NaNO_3$-KNO_3-KNO_2	1.783	1.63	1174
7	$LiNO_3$-KNO_3-$NaNO_2$-KNO_2	1.771	1.67	1183
8	$LiNO_3$-KNO_3-$NaNO_2$-$Mg(NO_3)_2$	1.782	1.68	1192
9	$LiNO_3$-$NaNO_3$-KNO_3-$Mg(NO_3)_2$-MgK	1.777	1.70	1242

The calculated energy density for each salt is given in Table 8. These values are significantly higher than that for thermal oils (59 MJ/m^3) [34], the best available ionic liquid (213 MJ/m^3) [35] and the solar salt ($NaNO_3$-KNO_3) (756 MJ/m^3) [18]. All the new synthesized salt mixtures have significantly higher energy density than solar salt and salt #3 shows the highest energy density among the new salts. Although salt #1 has higher heat capacity and good melting point, the energy density is still the lowest among new salt mixtures given by the effect of low density. The conclusion can be drawn from these observations that the energy density is a property affected by multiple parameters and every part plays an important role in determining the efficiency of energy storage of salt mixtures.

5. Conclusions

Experimental and theoretical investigations were conducted to determine physico-chemical properties of several LMP molten salts and energy storage density, in order to identify primary LMP molten salt candidates for TES systems.

The melting points of new generated thermal energy storage salts were experimentally determined using DSC. Different from metals, the melting point was chosen as the peak temperature rather than onset temperature of the endothermic peak due to the low thermal conductivity and broad phase transition range of the molten nitride salt mixture. All of the nine new thermal energy storage systems have melting points from 89°C to 124°C which are much lower than current sodium- potassium nitrate binary solar salt.

The heat capacity (C_p) of all the multi-component salts were also detected with DSC and found varying from 1.55 to 1.70 J/g.K at 500°C. The heat capacity in the liquid state increased linearly with increase in temperature.

Experimental measurements of density of multi-component systems were conducted as function of temperature in their liquid state and found the values were clustered in a very close range due to the similar composition. In liquid state, the density values decrease linearly as temperature increases. The results of those mixtures were compared to the solar salt and individual constituent salts. The comparison demonstrates the addition of lithium nitrate lowers the density, which is consistent with the observation that lithium nitrate has the lowest density among all the individual salts studied.

On the basis of density, heat capacity and the melting point, thermal energy storage was calculated and compared with thermal oil, ionic liquids and solar salts. The energy storage density of new TES molten salts studied are well above the all three thermal oil, ionic liquids and the current solar salt. All salt mixtures have melting temperatures in the range of 89-124°C, and energy storage density from 1099 MJ/m^3 to 1242 MJ/m^3 which is a 45-64% improvement over the current solar salt (756 MJ/m^3). The larger thermal energy storage density value indicates the better energy storage capacity for solar power generation systems. Because of the large energy storage capacity, the new developed molten salt systems can be suitably used as heat transfer fluid for solar energy storage system.

Acknowledgements

The author is pleased to acknowledge the financial support from Department of Energy (DOE), Grant No. DE-FG36-08GO18153 and ACIPCO for this research project. The author greatly acknowledges the assistance of T. Wang and D.

Mantha with the paper preparation, experiments and analysis, and The University of Alabama for providing the computational and experimental facilities.

References

[1] M. Asplund, N. Grevesse, A. J. Sauval, The new solar abundances - Part I: the observations, Communications in Asteroseismology, 2006, 147, p. 76–79.

[2] D. R. Williams, Sun Fact Sheet, NASA, 2004, http://nssdc.gsfc.nasa.gov/planetary/factsheet/sunfact.html

[3] U. Herrmann, Survey of Thermal Energy Storage for Parabolic Trough Power Plants, Journal of Solar Energy Engineering, 2002, 124, p 145 – 152.

[4] A. Steinfeld, R. Palumbo, Solar thermochemical process technology, Encyclopedia of Physical Science and Technology, 2001, p 237-256.

[5] E. A. Fletcher, Solarthermal processing: a review, Journal of Solar Energy Engineering, 2001, p 63-74.

[6] O.S. Lieberg, High Temperature Water Systems, The Industrial Press, New York, N.Y, USA, 1958, pp. 1-10.

[7] C. P. Fredlake et al., *J. Chem. Eng. Data*, 2004, 49, p 954-964.

[8] M. Zhang and R. G. Reddy, Solar Energy Materials II, Ed F. Dogan, M. Awano, D. Singh, and B. Tuttle, Materials Science and Technology (MS&T), (ISBN-13: 978-0-87170-866-3), 2007 p 151-160.

[9] L. Moens et al., *Transactions of the ASME*, 2003, 125, p 112-116.

[10] R. G. Reddy, Z. Zhang, M. F. Arenas and D. M. Blake, *High Temperature Materials and Processes*, 2003, 22, p 87-94.

[11] M. F. Arenas and R. G. Reddy, *Journal of Mining and Metallurgy*, B, 2003, 39 (1-2), p 81-91.

[12] A. P. Fraas and M. N. Ozisik, Heat Exchanger Design, John Wiley & Sons, Inc., New York, 1965, p 223-240.

[13] R. N. Lyon, et al., *Liquid Metals Handbook*, ONR, AEC, Bureau of Ships, Supt. of Documents, Wash. D.C., June 1952.

[14] C. B. Jackson, et al., *Liquid Metals Handbook*, Sodium-NaK Supplement, July 1955.

[15] H. G. MacPherson, et al., Molten-Salt Reactor Program Quarterly Progress Report for Period Ending July 31, 1960, ORNL-3014, Oak Ridge National Laboratory, USAEC.

[16] W. L. R. Emmet, "The Emmet Mercury Vapor Process," Trans. ASME, 1924, 46, p 253-261.

[17] W. E. Kirst, W.M. Nagle, and J.B. Cartner, "A New Heat Transfer Medium for High Temperatures," Trans. AIChE, 1940, 36, p 371-378.

[18] "Survey of Thermal Storage for Parabolic Trough Power Plants", Prepared by Pilkington Solar International for National Renewable Energy Laboratory, Subcontract No. AAR-9-29442-05, May 2000, p 12-16.

[19] N. A. Gokcen and R. G. Reddy (Authors), Thermodynamics, Plenum Publ., New York, N.Y., USA, 1996.

[20] G. J. Janz, Thermodynamic and Transport Properties of Molten Salts: Correlation Equations for Critically Evaluated Density, Surface Tension, Electrical Conductance and Viscosity Data, Journal of Physical and Chemical Reference Data, 17 (Suppl. 2), 1988, p 1-310.

[21] A. T. Ward, G. J. Janz, Molten Carbonate Electrolytes: Electrical Conductance, Density and Surface Tension of Binary and Ternary, Eleclrochimica Acta, 1965, 10, p 849-857.

[22] M. Zhang, R. G. Reddy, Thermodynamic properties of C4mim[Tf2N] ionic liquids, Mineral Processing and Extractive Metallurgy, 2010, 2, p 71-76.

[23] D. Mantha, T. Wang, R. G. Reddy, Thermodynamic Modeling of Eutectic Point in the LiNO3-NaNO3-KNO3 Ternary System, Journal of Phase Equilibria and Diffusion, (on-line) DOI: 10.1007/s11669-012-0005-4, 2011

[24] R. G. Reddy, T. Wang, D. Mantha, Thermodynamic properties of novel low melting point eutectic mixture in the $LiNO_3$–$NaNO_3$–KNO_3–$2KNO_3.Mg(NO_3)_2$ system for solar thermal energy storage, Thermochimica Acta, (2012), (sumbitted)

[25] T. Wang, D. Mantha, R. G. Reddy, Thermal stability of the eutectic composition in $LiNO_3$–$NaNO_3$–KNO_3 ternary system used for thermal energy storage, Solar Energy Materials and Solar Cells, (on line) DOI: 10.1016/j.solmat.2012.01.009, 2012.

[26] G. D. Carvalho, E. Frollini, W. N. D. Santos, Thermal conductivity of polymers by hot – wire method, Journal of Applied Polymer Science, 1996, 62, p 2281–2285.

[27] H. Bloom, A. Doroszkowski, S. B. Tricklebank, Molten salt mixtures. IX. The thermal conductivities of molten nitrate systems, Australian Journal of Chemistry, 1965, 18(8), p 1171–1176.

[28] A. G. Turnbull, Thermal conductivity of molten salts, Australian Journal of Applied Science, 1961, p1230-1241.

[29] L. R. White, H. T. Davis, Thermal conductivity of molten alkali nitrates, Journal of Chemical Physics, 1967, 47, p5433–5439

[30] M. V. Peralta-Martinez, M. J. Assael, M. J. Dix, L. Karagiannidis, W. A. Wakeham, A Novel Instrument for the Measurement of the Thermal Conductivity of Molten Metal. Part1: Instrument's Description, International Journal of Thermophysics, 2006, 27, p353–375.

[31] Y. Tada, M. Harada, M. Tanlgakl, W. Eguchl, Laser Flash Method for Measuring Thermal Conductivity of Liquids: Application to Molten Salts, Industrial and Engineering Chemistry Fundamentals, , 1981, 20, p333– 336.

[32] M. V. Smirnov, V. A. Khokhlov, E. S. Filatov, Thermal conductivity of molten alkali halides and their mixtures, Electrochimica Acta, 1986, 32, p1019–1026.

[33] G. P. Smith, G. F. Petersen, Volumetric Properties of the Molten System (Li,K)-(Cl,NO_3). Journal of Chemical Engineering Data, 1961, 6 (4), p 493-496.

[34] E. F. Camacho, M. Berenguel and F.R. Rubio, Advanced Control of Solar Plants, Springer-Verlag London Limited, London, UK, 1997, p.33-34.

[35] M. Zhang and R. G. Reddy, Solar Energy Maaterials II, Ed F. Dogan, M. Awano, D. Singh, and B. Tuttle, Materials Science and Technology (MS&T (ISBN-13: 978-0-87170-866-3), 2007, p 151-160.